doi.org/10.36721/PJPS.2026.39.11.311.1

miR-185 influences Cdc42-N-WASP signaling pathway in gastric cancer by targeting CTTN

Da Lian[1], Chengyao Bai[2], Xiaomeng Zhang[3], Xia Hou[2], Qingtian Wu[3] and Pengyu Xie[2*]

[1]Jiamusi University School of Clinical Medicine, Jiamusi, Heilongjiang, 154100, China
[2]Department of Genetics, Jiamusi University School of Basic Medicine, Jiamusi, Heilongjiang, 154007, China
[3]Jiamusi University School of Basic Medicine, Jiamusi, Heilongjiang, 154007, China

Abstract: **Background**: miR-185 expression is dysregulated in various tumors, but its role in gastric cancer remains unclear. **Objectives**: To investigate miR-185 expression and clinical significance in gastric cancer, explore its effects on malignant phenotypes and preliminarily elucidate the underlying mechanism. **Methods**: Real-time polymerase chain reaction (PCR) was used to detect miR-185 expression in 58 archived gastric cancer tissue samples and paired adjacent normal tissues obtained from a hospital biospecimen repository. In SGC-7901 and AGS cells, the effects of miR-185 modulation on proliferation, apoptosis, epithelial-mesenchymal transition (EMT) and the cell division cycle protein 42 (Cdc42)-neural Wiskott-Aldrich syndrome protein (N-WASP) pathway were assessed using 5-ethynyl-2′-deoxyuridine (EdU) assay, flow cytometry, Western blot and dual-luciferase reporter assay. **Results**: miR-185 expression was significantly downregulated in gastric cancer tissues and correlated with lymph node metastasis and advanced stage. *In vitro, miR-185 overexpression inhibited proliferation, induced apoptosis, increased E-cadherin expression and decreased Vimentin, N-cadherin, Snail, Cdc42 and* neural WASP expression. A dual-luciferase reporter assay confirmed that cortactin (CTTN) is a direct target of miR-185. These findings were consistent in both cell lines. **Conclusion**: miR-185 is downregulated in gastric cancer and its low expression correlates with lymph node metastasis and advanced TNM stage. *In vitro experiments indicate that upregulation of miR-185 suppresses gastric cancer cell proliferation, induces apoptosis and reverses epithelial-mesenchymal transition, possibly by* targeting CTTN and thereby affecting Cdc42 and N-WASP expression. This single-center, small-sample (n=58) *in vitro study lacks in vivo* validation; the findings require confirmation in larger, multicenter cohorts. Nevertheless, this study provides the first experimental evidence for the miR-185/CTTN/Cdc42-N-WASP axis in gastric cancer.

Keywords: Cortactin; Epithelial-mesenchymal transition; Gastric cancer; miR-185; Proliferation

Submitted on 19-11-2025 – Revised on 12-05-2026 – Accepted on 02-06-2026

INTRODUCTION

Gastric cancer is one of the most common malignant tumors worldwide and poses a serious threat to human health. The burden of gastric cancer in China is particularly severe, with an incidence rate of approximately 25.41 per 100,000 people in 2022 (Chen *et al*., 2025). However, due to population aging, the total number of gastric cancer cases is expected to increase by 62% over the next 20 years (Chen, 2024). Therefore, exploring the molecular mechanisms underlying gastric cancer development and identifying new diagnostic markers and therapeutic targets are of great clinical significance. miR-185 exerts tumor-suppressive effects in various malignancies and is involved in the regulation of tumor cell proliferation, invasion and epithelial-mesenchymal transition (EMT). Previous studies have shown that miR-185 inhibits tumor progression in gastrointestinal cancers by targeting multiple downstream genes (Babaeenezhad *et al*., 2022). However, the role and molecular mechanism of miR-185 in gastric cancer remain unclear.

CTTN (cortactin) is an important member of the cortactin-binding protein family and is involved in regulating cytoskeletal rearrangement and pseudopodia formation. In various tumors, CTTN overexpression is closely associated with tumor invasion and metastasis. The Cdc42-N-WASP signaling pathway is a core pathway regulating cytoskeletal rearrangement and pseudopodia formation. Cdc42, an important member of the Rho family of small GTPases, activates its downstream effector N-WASP, which in turn activates the Arp2/3 complex, mediating actin polymerization and cytoskeletal rearrangement (Hasegawa *et al*., 2022). Previous studies have shown that CTTN interacts with Cdc42 and N-WASP to coordinate cytoskeletal rearrangement. In tumor cells, this pathway promotes tumor cell invasion and metastasis; for example, in colorectal cancer, LASP1 interacts with N-WASP to activate Arp2/3, thereby promoting tumor invasion and metastasis (Zheng *et al*., 2023). However, whether miR-185 regulates the Cdc42-N-WASP signaling pathway by targeting CTTN, thereby affecting gastric cancer cell proliferation, apoptosis and EMT, remains unreported.

To test this hypothesis, miR-185 expression was measured in gastric cancer tissues and its clinical significance was analyzed, CTTN was validated as a direct target of miR-185 and the effects of this regulatory axis on the malignant phenotypes of gastric cancer cells were investigated. This study aims to elucidate the role and

**Corresponding author:* e-mail: xiepengyu@jmsu.edu.cn

molecular mechanism of miR-185 in gastric cancer, providing a potential new target for gastric cancer therapy.

MATERIALS AND METHODS

Research object

A total of 58 archived gastric cancer tissue samples and paired adjacent normal tissue samples were obtained from the biospecimen repository of Jiamusi University School of Basic Medicine. These samples were derived from patients who underwent total or subtotal gastrectomy. The cohort comprised 32 males and 26 females, aged 38–72 years, with a mean age of 52.5 ± 9.5 years. Pathological diagnosis and TNM staging were performed in the pathology department during surgery.

Inclusion criteria were: (1) first-time pathological diagnosis of primary gastric cancer; (2) no prior surgery, radiotherapy, or chemotherapy; (3) complete clinicopathological data.

Exclusion criteria were: (1) recurrent or metastatic gastric cancer; (2) previous surgery or other treatments; (3) concurrent other tumors or metabolic diseases at admission. Clinical staging followed the TNM staging criteria for gastric cancer promulgated by the International Union Against Cancer (UICC) in 2018 (Fang *et al*., 2018): 12 cases stage I, 17 stage II, 11 stage III and 18 stage IV. Tumor differentiation: 18 cases of well-differentiated adenocarcinoma, 19 moderately differentiated, 12 poorly differentiated and 9 undifferentiated. Lymph node metastasis was present in 39 cases. All tissue samples were stored at −80°C after collection.

The ethics committee granted a waiver of informed consent for the use of archived de-identified tissue samples. This study was conducted in accordance with the principles of the Declaration of Helsinki. Sample size estimation was based on the expected difference in miR-185 expression between gastric cancer and adjacent normal tissues from previous studies (Shahabi *et al*., 2021; effect size d = 0.8), with $\alpha = 0.05$ (two-sided) and power $(1-\beta) = 0.80$. Using the formula for two-sample mean comparison, at least 26 cases per group were required. A total of 58 samples were finally included.

Materials and instruments

Gastric cancer cell lines SGC-7901 and AGS were maintained in culture in our laboratory. PVDF membranes were purchased from Pall Life Sciences, ECL reagents were purchased from Amersham Biosciences and monoclonal antibodies against CTTN, Cdc42 and N-WASP and HRP-labeled IgG were purchased from Cell Signaling Technology (USA). RNA extraction and reverse transcription kits were purchased from Axygen (USA). miR-185 mimics, miR-185 inhibitors and corresponding negative controls were synthesized by Shanghai Gemma Pharmaceutical Technology Co., LTD. (China). SGC-7901 and AGS cell lines were purchased from the Cell Bank of the Committee for Typical Culture Collection, Chinese Academy of Sciences (Shanghai), with catalog numbers of TChu 182 and SCSP-503, respectively. "In all experiments, cells from passages 5 to 15 were used for both cell lines." Short tandem repeat (STR) identification was performed to verify the identity of the two cell lines. STR profiling confirmed that SGC-7901 and AGS cell lines were consistent with their respective reference profiles, showing 100% match at all tested loci.

Cell culture and grouping

SGC-7901 and AGS cells were cultured in RPMI 1640 medium supplemented with 10% fetal bovine serum and 1% penicillin-streptomycin at 37°C in a 5% CO_2 incubator (Heracell VIOS 160i, Thermo Fisher Scientific, USA) (Lu *et al*., 2023). Cells in the logarithmic growth phase were used for experiments and divided into three groups: a control group, a miR-185 mimics group and a miR-185 inhibitor group.

Transfection

miR-185 mimics, a double-stranded RNA used to overexpress miR-185, had the following sequences: guide strand (mature strand) 5‘-UGGAGAGAA AGGCAGUUCCUGA-3’ (hsa-miR-185-5p) and passenger strand 5‘-UCCUGGAGGAUCUCUAUACGU-3’. Both strands were modified with 2‘-O-methylation to enhance stability and phosphorothioate linkages at the 3’ end to increase nuclease resistance. The miR-185 inhibitor, a chemically modified single-stranded antisense oligonucleotide used to inhibit endogenous miR-185 expression specifically, had the sequence 5‘-UCCUGGAGGAUCUCUAUACGU-3’, fully complementary to the mature miR-185 sequence and was modified with 2‘-O-methylation and phosphorothioate linkages. Negative controls were scrambled oligonucleotides with no homology to the human genome, including NC mimics (double-stranded) and NC inhibitor (single-stranded). All oligonucleotides were purified by high-performance liquid chromatography (HPLC) and had purity >95%.

Cells were seeded in 6-well plates (2×10^5 cells/well) and cultured to 70%–80% confluence. Transfection was performed using Lipofectamine 2000 (Invitrogen, USA) according to the manufacturer’s instructions. miR-185 mimics, miR-185 inhibitor, or corresponding negative controls were added at a final concentration of 50 nM. Cells were harvested 48 hours after transfection for subsequent experiments (Bao *et al*., 2024).

Transfection efficiency was assessed in parallel experiments using FAM-labeled negative controls under the same transfection conditions. At 24 hours post-transfection, the proportion of FAM-positive cells was assessed by fluorescence microscopy (Olympus, Japan) and quantified by flow cytometry (BD FACSCalibur, USA). Transfection efficiency was calculated as the percentage of FAM-positive cells among total cells. Only

experiments with transfection efficiency > 80% were used for further analysis.

Real-time quantitative PCR for miRNA expression

Total RNA, including small RNA fractions, was extracted from tissue and cell samples using the miRNeasy Mini Kit (Qiagen, Germany). RNA concentration and purity were measured using a NanoDrop 2000 (Thermo Fisher Scientific, USA). Reverse transcription for miRNA was performed using the Mir-X miRNA First-Strand Synthesis Kit (TaKaRa, Japan): 1 μg of total RNA was added to 2× miRNA Reaction Buffer and PrimeScript Enzyme Mix, using stem-loop reverse transcription primers for miR-185 and U6 internal control primers. The reaction conditions were 37°C for 60 minutes, followed by 85°C for 5 seconds (Bao *et al*., 2024).

Real-time quantitative PCR was performed using SYBR Green Master Mix (TaKaRa, Japan) on an ABI 7500 Real-Time PCR System (Applied Biosystems, USA). The primer sequences used for miR-185, U6, CTTN, E-cadherin, Vimentin and GAPDH are listed in table 1. The reaction mixture consisted of 10 μL of 2× SYBR Green Master Mix, 0.5 μL of miR-185-specific forward primer (5‘-TGGAGAGAAAGGCAGTTCC-3’), 0.5 μL of universal reverse primer, 2 μL of cDNA template and ddH_2O to a final volume of 20 μL. The PCR conditions were: 95°C for 30 seconds, followed by 40 cycles of 95°C for 5 seconds and 60°C for 34 seconds. Melt curve analysis was performed to verify amplification specificity. U6 snRNA was used as an internal control, with forward primer 5‘-CTCGCTTCGGCAGCACA-3’ and reverse primer 5‘-AACGCTTCACGAATTTGCGT-3’.

Relative miR-185 expression was calculated using the $2^{-}\Delta\Delta Ct$ method. $\Delta Ct = Ct(miR\text{-}185) - Ct(U6)$. $\Delta\Delta Ct = \Delta Ct(experimental\ sample) - \Delta Ct(calibrator\ sample)$. Adjacent normal tissues or negative control cells were used as calibrator samples, with their expression set to 1.00. All samples were tested in triplicate and the experiments were independently repeated three times.

MTT assay

Cells were seeded in 96-well plates (5×10^3 cells/well) and transfected as described above. At 48 hours post-transfection, 20 μL of MTT solution (5 mg/mL) was added to each well and the plate was incubated for 4 hours. The supernatant was carefully removed and 150 μL of dimethyl sulfoxide was added to dissolve the formazan crystals. Absorbance was measured at 570 nm using a microplate reader (Bio-Rad, USA). Each group was tested in triplicate and the experiment was independently repeated three times (Castro-Guijarro *et al*., 2022).

EdU incorporation assay

SGC-7901 cells were seeded in 96-well plates (5×10^3 cells/well) and transfected with miR-185 mimics, miR-185 inhibitor, or negative controls. At 48 hours post-transfection, the EdU assay was performed using an EdU Cell Proliferation Detection Kit (RiboBio, China) according to the manufacturer‘s instructions. Cells were incubated with EdU working solution (final concentration 10 μmol/L) for 2 hours, fixed with 4% paraformaldehyde for 15 minutes, permeabilized with 0.5% Triton X-100 for 10 minutes, stained with Apollo reaction solution for 30 minutes in the dark and counterstained with Hoechst 33342 for 5 minutes. Images were captured using a fluorescence microscope (BX53, Olympus, Japan) at 200× magnification and five random fields per group were selected for analysis (Tian *et al*., 2025). The EdU-positive cell rate was calculated as the percentage of EdU-positive cells among Hoechst-stained total cells. Each group was tested in triplicate and the experiment was independently repeated three times.

Caspase-3 activity assay

At 48 hours post-transfection, cells were harvested and Caspase-3 activity was measured using a Caspase-3 Activity Assay Kit (Beyotime, China) according to the manufacturer’s instructions. Cells were lysed on ice for 15 minutes, centrifuged at 20,000 × g for 5 minutes at 4°C and the supernatant was collected. The reaction was initiated by adding 2 mM Ac-DEVD-pNA substrate and after incubation at 37°C for 2 hours, absorbance was measured at 405 nm (Wang *et al*., 2021). Incubation operations were performed in a (Heracell VIOS 160i CO2 incubator (Heracell VIOS 160i, Thermo Fisher Scientific, USA), Thermo Fisher Scientific, USA) incubator and absorbance readings were acquired using a (Synergy H1 Multifunctional microplate Reader, BioTek Instruments, USA) microplate reader. Each group was tested in triplicate and the experiment was independently repeated three times.

Annexin V/PI double staining flow cytometry

SGC-7901 and AGS cells were seeded in 6-well plates (2×10^5 cells/well) and transfected as described. At 48 hours post-transfection, cells were harvested and stained using an Annexin V-FITC/PI Apoptosis Detection Kit (BD Biosciences, USA). Cells were washed twice with PBS, resuspended in 1× Binding Buffer at a density of 1×10^6 cells/mL and 100 μL of cell suspension (1×10^5 cells) was mixed with 5 μL of Annexin V-FITC and 5 μL of PI (Tian *et al*., 2025). After incubation at room temperature in the dark for 15 minutes, 400 μL of 1× Binding Buffer was added and the samples were analyzed within 1 hour using a flow cytometer (BD FACSCalibur, USA). Data were analyzed using FlowJo software (Version 10.8.1, FlowJo LLC, Ashland, OR, USA). Early apoptotic cells were Annexin V-positive/PI-negative, late apoptotic cells were Annexin V-positive/PI-positive and necrotic cells were Annexin V-negative/PI-positive. The total apoptosis rate was calculated as the sum of early and late apoptotic rates. Each group was tested in triplicate and the experiment was independently repeated three times.

Western blot

At 48 hours post-transfection, cells were harvested and lysed in RIPA buffer containing protease inhibitors

(Roche, Switzerland) on ice for 30 minutes. After centrifugation at 12,000 rpm for 15 minutes at 4°C, the supernatant was collected as the total protein fraction. Protein concentration was determined using a BCA Protein Assay Kit (Thermo Fisher Scientific, USA). Equal amounts of protein (30 μg per lane) were separated by 10% SDS-PAGE and transferred onto PVDF membranes ((Immobilon-P, Millipore, USA) by wet transfer (Wang *et al*., 2022a). Membranes were blocked with 5% non-fat milk in TBST for 1 hour at room temperature and then incubated overnight at 4°C with primary antibodies against CTTN (1:1000, #4562), Cdc42 (1:1000, #2466), N-WASP (1:1000, #4848), E-cadherin (1:1000, #3195), Vimentin (1:1000, #5741), Snail (1:1000, #3879) and GAPDH (1:2000, #5174) (all from Cell Signaling Technology, USA). After washing with TBST three times, membranes were incubated with HRP-conjugated goat anti-rabbit secondary antibody (1:5000, Cell Signaling Technology, USA) for 1 hour at room temperature. Protein bands were visualized using enhanced chemiluminescence (ECL) reagents (Amersham ECL Prime, Cytiva,, USA) and imaged with a ChemiDoc XRS+ system (Bio-Rad, USA). Densitometric analysis was performed using ImageJ software (NIH, USA). Relative protein expression was normalized to GAPDH and the negative control group was set to 1.00. Each experiment was independently repeated three times.

Dual-luciferase reporter assay

The binding sites between miR-185 and the 3‘UTR of CTTN were predicted using TargetScan and miRDB databases. The CTTN 3’UTR fragment containing the predicted binding site was amplified by PCR and cloned into the pmirGLO dual-luciferase reporter vector (Promega, USA) to construct the wild-type recombinant plasmid (CTTN-3‘UTR-WT). A mutant recombinant plasmid (CTTN-3’UTR-MUT) was generated by site-directed mutagenesis using overlapping extension PCR and all plasmids were verified by sequencing.

293T cells were seeded in 24-well plates (8×10^4 cells/well) and co-transfected using Lipofectamine 2000 (Invitrogen, USA) with 0.5 μg of reporter plasmid (CTTN-3‘UTR-WT or MUT), 50 nM miR-185 mimics or negative control and 0.1 μg of pRL-TK internal control plasmid (Promega, USA). After 48 hours, luciferase activity was measured using a Dual-Luciferase Reporter Assay Kit (Promega, USA) according to the manufacturer’s instructions (Hou *et al*., 2021). Relative luciferase activity was calculated as firefly luciferase activity / Renilla luciferase activity. Each group was tested in triplicate and the experiment was independently repeated three times.

Comparison of baseline miR-185 expression in normal gastric epithelial cells and gastric cancer cells

The human normal gastric epithelial cell line GES-1 was purchased from the Cell Bank of the Chinese Academy of Sciences (Shanghai, China). GES-1 cells were cultured in RPMI 1640 medium containing 10% fetal bovine serum. Total RNA was extracted from GES-1, SGC-7901 and AGS cells in the logarithmic growth phase using TRIzol reagent (Invitrogen, USA). Real-time quantitative PCR was performed as described above to detect miR-185 expression, with U6 as an internal control. Expression levels were normalized to GES-1 (set to 1.00). Each group was tested in triplicate and the experiment was independently repeated three times.

Construction of CTTN overexpression plasmid and functional rescue experiment

The human CTTN coding region (CDS) was amplified by PCR and cloned into the pcDNA3.1(+) eukaryotic expression vector (Invitrogen, USA) to construct the CTTN overexpression plasmid (pcDNA3.1-CTTN). The plasmid was verified by sequencing and the empty vector pcDNA3.1 was used as a negative control. SGC-7901 cells were seeded in 6-well plates (2×10^5 cells/well) and co-transfected using Lipofectamine 2000 (Invitrogen, USA) in the following groups: (1) NC mimics + Vector group: co-transfected with 50 nM NC mimics and 1.0 μg empty vector; (2) miR-185 mimics + Vector group: co-transfected with 50 nM miR-185 mimics and 1.0 μg empty vector; (3) miR-185 mimics + CTTN group: co-transfected with 50 nM miR-185 mimics and 1.0 μg pcDNA3.1-CTTN; (4) NC mimics + CTTN group: co-transfected with 50 nM NC mimics and 1.0 μg pcDNA3.1-CTTN. After 48 hours, cells were collected for subsequent assays, including Western blot for CTTN, Cdc42, N-WASP, E-cadherin and Vimentin; MTT assay for cell proliferation; EdU assay for DNA synthesis; and Annexin V/PI flow cytometry for apoptosis.

Validation in another gastric cancer cell line

To confirm the generalizability of the findings, key experiments were repeated in the AGS gastric cancer cell line, including cell transfection, real-time quantitative PCR, Western blot and MTT assay. The experimental methods were the same as those used for SGC-7901 cells.

Statistical analysis

All data were analyzed using SPSS 26.0 software (IBM, USA). Continuous data are presented as mean ± standard deviation (SD). Normality was assessed using the Shapiro–Wilk test and homogeneity of variances was assessed using Levene‘s test. Comparisons between paired samples were performed using paired t-test (if normally distributed) or a Wilcoxon signed-rank test (if not normally distributed). For two-group comparisons, independent samples t-test (if normally distributed and homogeneous variances) or Mann–Whitney U test (if not) was used. For multiple-group comparisons, one-way analysis of variance (ANOVA) (if normally distributed and homogeneous variances) or Kruskal–Wallis H test (if not) was used. Post hoc multiple comparisons following ANOVA were performed using Tukey’s test and following Kruskal–Wallis H test using Dunn‘s test with Bonferroni correction.

Table 1: Primer sequences.

Gene	Forward 5'-3'	Reverse 5'-3'
miR-185	TGGAGAGAAAGGCAGTTCC	Universal reverse primer
U6	CTCGCTTCGGCAGCACA	AACGCTTCACGAATTTGCGT
CTTN	CTAGATATACGACGTGGAT	TATTAGACTGAGATTAGATG
E-cadherin	TAAGGAAAGCGGAATG	ACCTATTCTATCATCTTGT
Vimentin	CAACCGCTCCTAGCTTAAG	GCACGATTGACTGCTTTGTGA
GAPDH	AGTACCAGTCTGGCTGG	TAATAGACGGATGTCTGGT

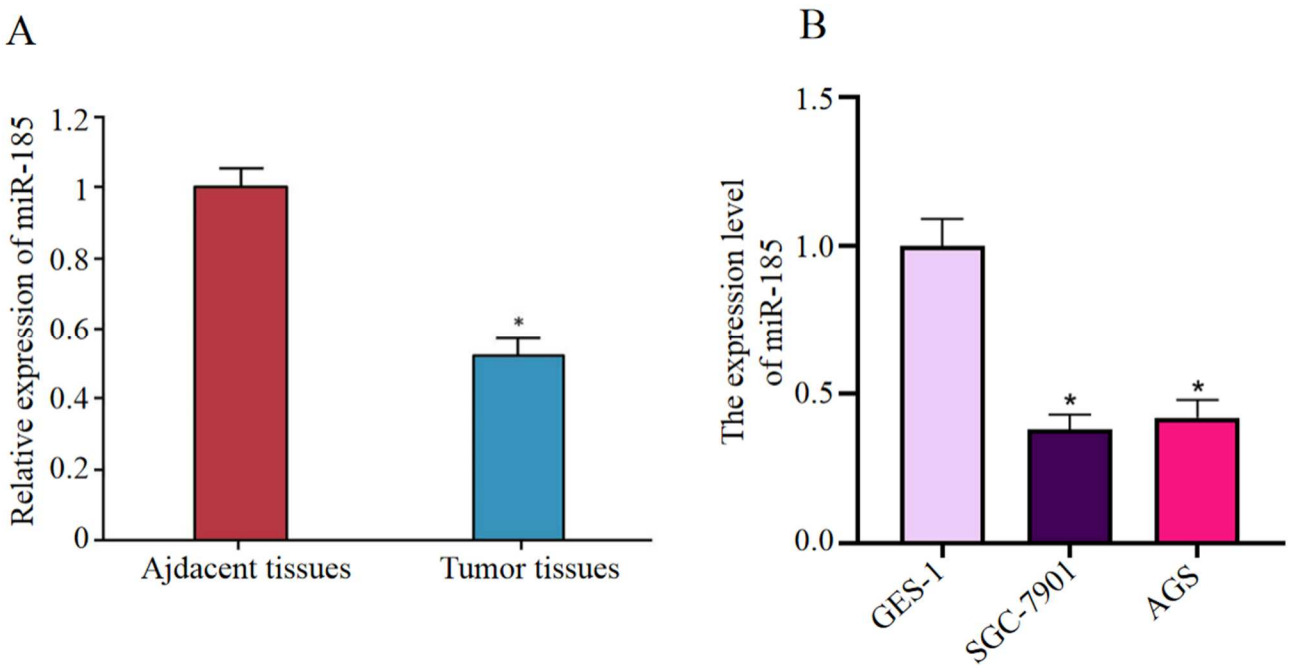

Fig. 1: Comparison of baseline miR-185 expression.
(A) Real-time quantitative PCR analysis of miR-185 expression in gastric cancer tissues (n = 58) and paired adjacent normal tissues (n = 58). U6 was used as an internal control, and adjacent tissues were used as calibrators (set to 1.00); (B) Real-time quantitative PCR analysis of miR-185 expression in GES-1 (normal gastric epithelial cells), SGC-7901, and AGS (gastric cancer cells). U6 was used as an internal control and expression was normalized to GES-1 (set to 1.00). Data are presented as mean ± SD. **P* < 0.05 vs. adjacent tissues/GES-1. (A) Paired t-test; (B) One-way ANOVA followed by Tukey's post hoc test.

For correlations between miR-185 expression and clinicopathological parameters, Spearman's rank correlation coefficient was used for ordinal variables (e.g., TNM stage, differentiation grade). Pearson's correlation coefficient was used for continuous variables (e.g., age, BMI) when they were normally distributed; otherwise, Spearman's rank correlation coefficient was used. All correlation analyses reported the correlation coefficient (*r* or ρ), the 95% confidence interval and the P value. Patients were dichotomized into high and low miR-185 expression groups based on the median expression level and group comparisons were performed using the χ^2 test or Fisher's exact test. All tests were two-sided and $P < 0.05$ was considered statistically significant. For multiple comparisons, $P < 0.05$ corrected for multiple comparisons was considered significant.

RESULTS

miR-185 expression in gastric cancer

Real-time quantitative PCR was used to detect miR-185 expression in gastric cancer tissues and paired adjacent normal tissues. Using U6 as an internal control and adjacent tissues as calibrators (set to 1.00), relative expression was calculated by the $2^{-}\Delta\Delta Ct$ method. Paired t-test showed that miR-185 expression was significantly lower in gastric cancer tissues than in paired adjacent normal tissues (0.38 ± 0.05 vs. 1.00 ± 0.09, mean difference = −0.62, *95% CI*: −0.78 to −0.46, $P < 0.001$) (Fig. 1A). To determine whether the change in miR-185 expression was tumor-specific, baseline miR-185 levels were measured in the normal gastric epithelial cell line GES-1. miR-185 expression in SGC-7901 and AGS gastric cancer cells was 0.38 ± 0.05-fold and 0.42 ± 0.06-fold that of GES-1 cells, respectively, both statistically significant ($P < 0.05$) (Fig. 1B).

Table 2: Correlation between miR-185 expression and clinicopathological characteristics.

Parameter	*n*	*Spearman ρ*	*95% CI*	*P*
Age (years)	58	0.113	-0.148 ~ 0.362	0.398
BMI (kg/m²)	58	0.209	-0.054 ~ 0.447	0.115
TNM stage (I/II vs III/IV)	58	-0.721	-0.832 ~ -0.558	< 0.001
Tumor size (cm)	58	-0.589	-0.748 ~ -0.370	< 0.001
Lymph node metastasis (yes/no)	58	-0.715	-0.829 ~ -0.549	< 0.001
Differentiation (well/moderate vs poor/undifferentiated)	58	-0.618	-0.768 ~ -0.408	< 0.001

Note: miR-185 expression levels are presented as $2^{-}\Delta\Delta Ct$. Spearman's rank correlation test was used for age, BMI, TNM stage, tumor size, lymph node metastasis, and differentiation. The chi-square (χ^2) test was used for sex.

Association of miR-185 with clinicopathological characteristics

Spearman rank correlation analysis was used to assess the correlation between miR-185 expression and clinicopathological parameters. miR-185 expression was significantly negatively correlated with TNM stage (ρ = −0.721, *95% CI*: −0.832 to −0.558, $P < 0.001$), lymph node metastasis (ρ = −0.715, *95% CI*: −0.829 to −0.549, $P < 0.001$), tumor size (ρ = −0.589, *95% CI*: −0.748 to −0.370, $P < 0.001$) and tumor differentiation grade (ρ = −0.618, *95% CI*: −0.768 to −0.408, $P < 0.001$). No significant correlation was observed with patient age (ρ = 0.113, *95% CI*: −0.148 to 0.362, $P = 0.398$) or sex (χ^2 = 0.624, $P = 0.430$) (Table 2).

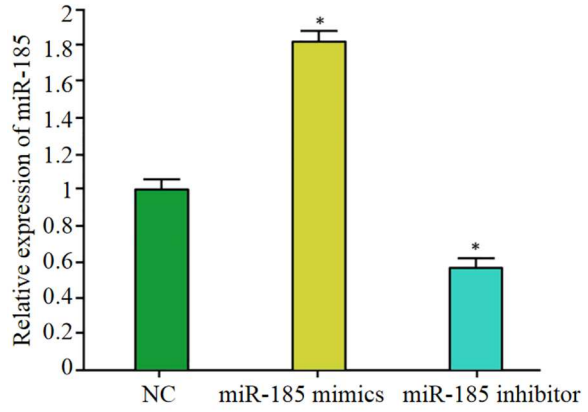

Fig. 2: Validation of miR-185 expression modulation efficiency.

Real-time quantitative PCR analysis of miR-185 expression in SGC-7901 cells after transfection with miR-185 mimics or miR-185 inhibitor. Data are presented as mean ± SD from three independent experiments. An independent-samples t-test was used to compare two groups. *$P < 0.05$ vs. control group.

Validation of miR-185 expression modulation efficiency

At 48 hours post-transfection, miR-185 expression levels in SGC-7901 and AGS cells were measured by stem-loop real-time quantitative PCR, with U6 as an internal control and the negative control group as calibrator (set to 1.00). Transfection with miR-185 mimics significantly increased miR-185 expression in SGC-7901 cells compared with the negative control group (8.42 ± 0.67-fold, $P < 0.05$), while transfection with miR-185 inhibitor significantly decreased its expression (0.31 ± 0.04-fold, $P < 0.05$) (Fig. 2).

Transfection efficiency and siRNA specificity validation

Fluorescence microscopy showed abundant FAM-positive cells in SGC-7901 and AGS cells 24 hours after transfection (Fig. 3A). Flow cytometry quantitative analysis indicated that the transfection efficiency was 86.5 ± 4.2% for SGC-7901 cells and 83.8 ± 5.1% for AGS cells (Fig. 3B, C), meeting the requirement for subsequent experiments (> 80%).

Effect of miR-185 on gastric cancer cell proliferation

MTT assay was used to evaluate the effect of miR-185 modulation on cell proliferation. In SGC-7901 cells, miR-185 mimics significantly inhibited cell proliferation, whereas miR-185 inhibitor significantly promoted cell proliferation ($P < 0.05$) (Fig. 4A). These results were further confirmed by EdU incorporation assay. In SGC-7901 cells, the EdU-positive cell rate was 42.6 ± 3.8% in the negative control group, significantly decreased to 18.3 ± 2.5% in the miR-185 mimics group ($P < 0.05$) and increased to 68.4 ± 5.2% in the miR-185 inhibitor group ($P < 0.05$) (Fig. 4B).

Effect of miR-185 on gastric cancer cell apoptosis

Caspase-3 activity was measured to assess apoptosis. In SGC-7901 cells, miR-185 mimics significantly increased Caspase-3 activity, while miR-185 inhibitor significantly decreased it ($P < 0.05$) (Fig. 5A). Annexin V/PI double staining flow cytometry further confirmed these findings. In SGC-7901 cells, the total apoptosis rate was 4.7 ± 1.1% in the negative control group, increased significantly to 25.4 ± 3.1% in the miR-185 mimics group ($P < 0.05$) and decreased to 2.7 ± 0.7% in the miR-185 inhibitor group ($P < 0.05$) (Fig. 5B).

Effect of miR-185 on epithelial-mesenchymal transition in gastric cancer cells

To investigate whether miR-185 regulates epithelial-mesenchymal transition (EMT) in gastric cancer cells, the expression of EMT-related markers was examined.

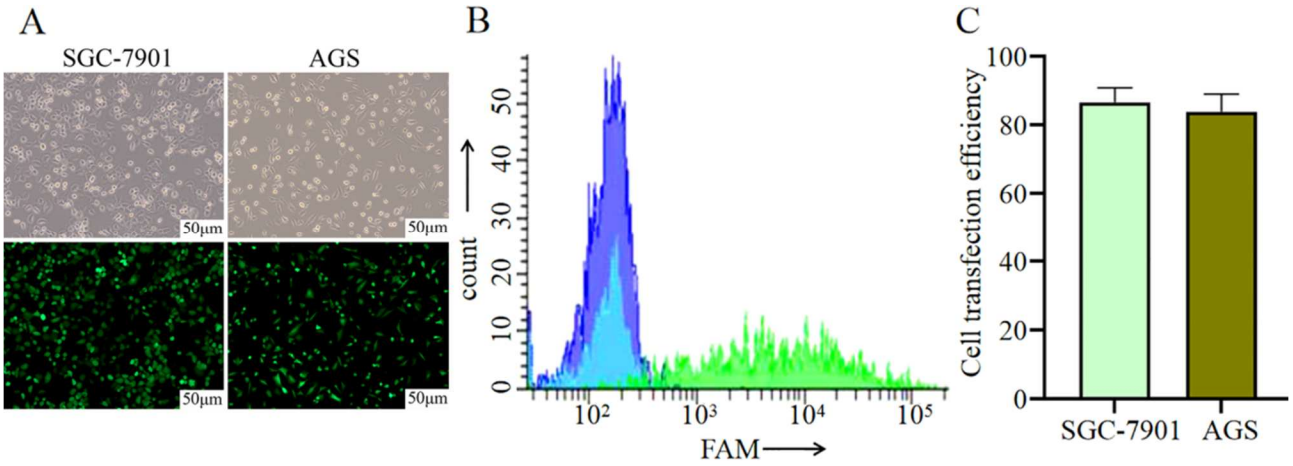

Fig. 3: Transfection efficiency validation.
(A) Fluorescence microscopy images of FAM-labeled negative control-transfected SGC-7901 cells showing FAM-positive cells (green fluorescence). Scale bar = 100 μm; (B) Representative flow cytometry histogram of transfection efficiency in SGC-7901 cells; (C) Quantitative analysis of transfection efficiency in SGC-7901 and AGS cells (n = 3, mean ± SD). Transfection efficiencies were 86.5 ± 4.2% for SGC-7901 and 83.8 ± 5.1% for AGS cells. No statistical comparisons were performed for transfection efficiency; values are descriptive only.

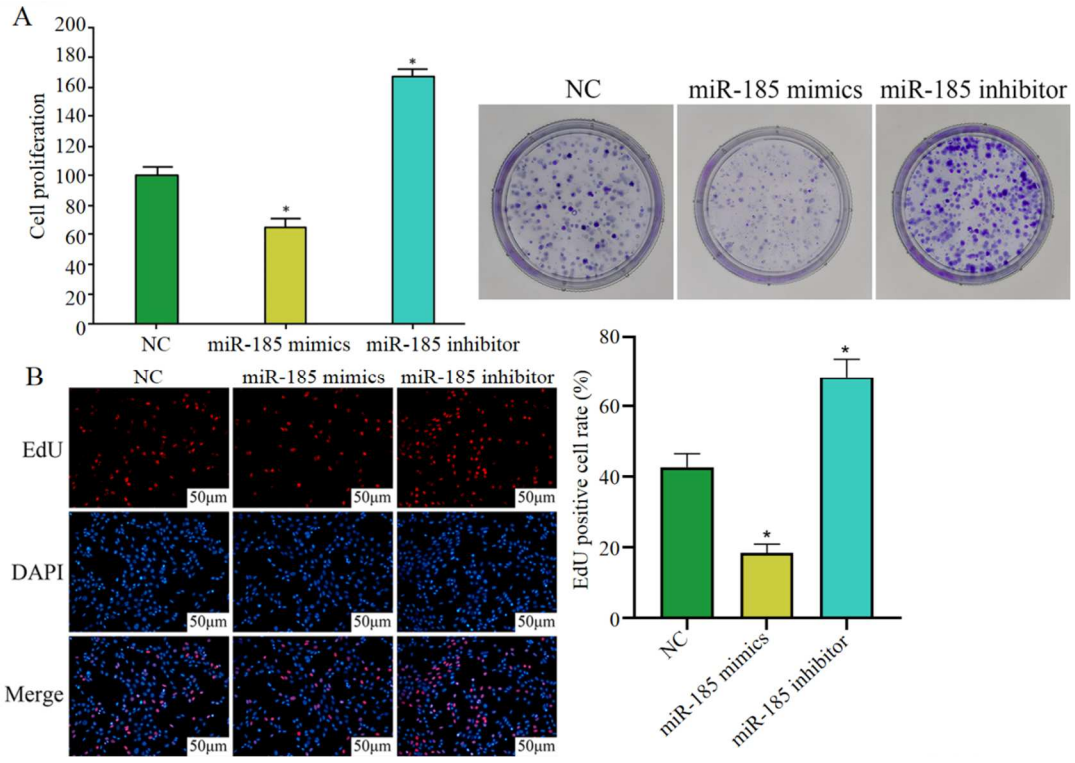

Fig. 4: Effect of miR-185 on gastric cancer cell proliferation.
(A) MTT assay analysis of cell proliferation in SGC-7901 cells after transfection with miR-185 mimics, miR-185 inhibitor, or negative controls (NC). Absorbance at 570 nm (A570) is shown. Data are presented as mean ± SD from three independent experiments. *P < 0.05 vs. NC group; (B) EdU incorporation assay analysis of DNA synthesis activity in SGC-7901 cells. Left panel: representative fluorescence images (EdU: red; Hoechst: blue). Right panel: quantitative analysis of EdU-positive cell rate. Scale bar = 50 μm. Data are presented as mean ± SD from three independent experiments. One-way ANOVA followed by Tukey's post hoc test was used for comparisons among the three groups (NC, miR-185 mimics, miR-185 inhibitor). *P < 0.05 vs. NC group.

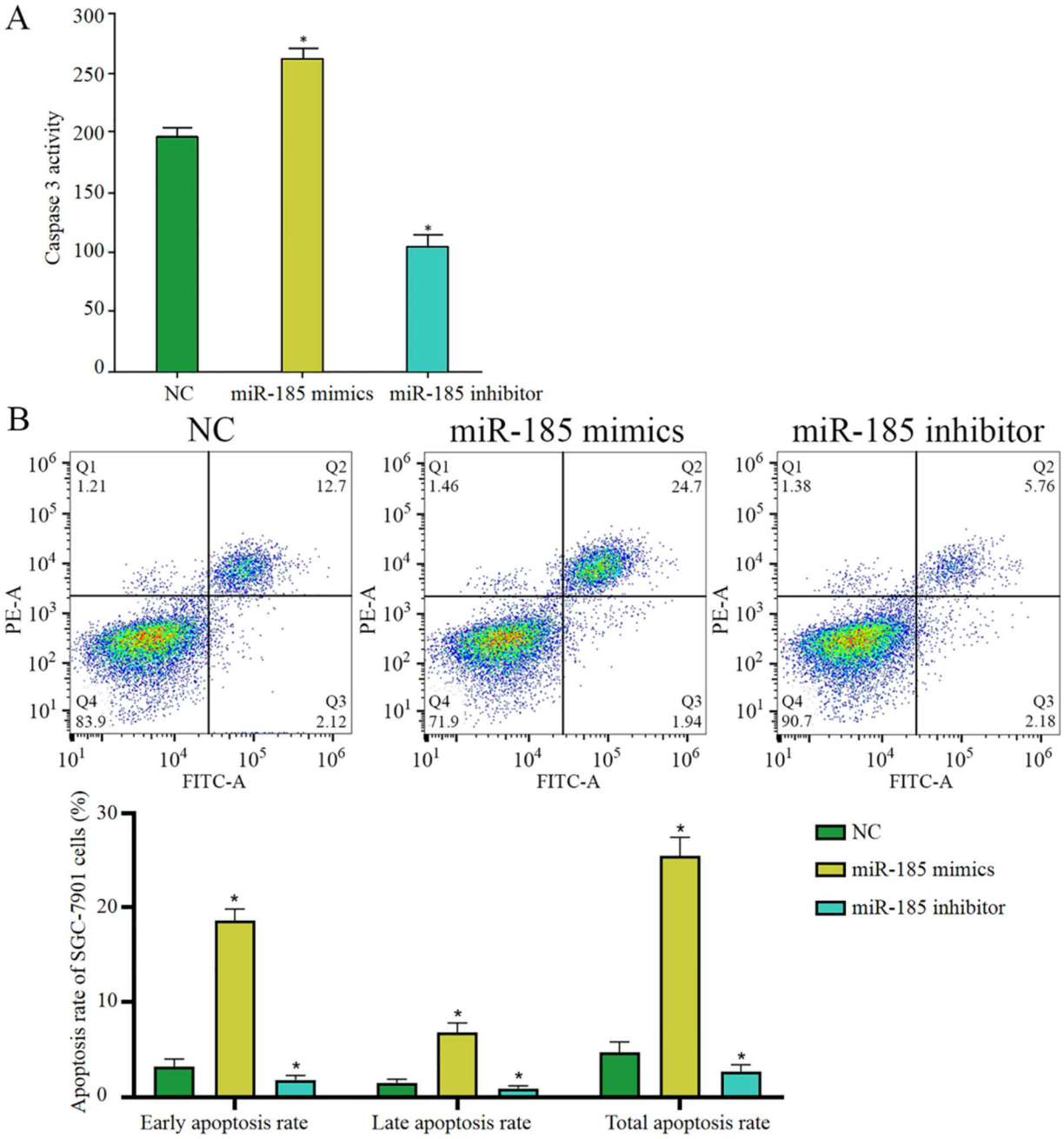

Fig. 5: Effect of miR-185 on gastric cancer cell apoptosis.
(A) Caspase-3 activity in SGC-7901 and AGS cells after transfection; (B) Annexin V/PI double staining flow cytometry analysis of apoptosis in SGC-7901 cells. Left panel: representative flow cytometry plots (Qa: necrotic cells; Qb: late apoptotic cells; Qc: early apoptotic cells; Qd: viable cells). Right panel: quantitative analysis of total apoptosis rate. Data are presented as mean ± SD from three independent experiments. One-way ANOVA followed by Tukey's post hoc test was used for comparisons among the three groups (NC, miR-185 mimics, miR-185 inhibitor). *$P < 0.05$ vs. NC group.

Real-time quantitative PCR results showed that in SGC-7901 cells, miR-185 mimics significantly upregulated the epithelial marker E-cadherin and significantly downregulated the mesenchymal markers Vimentin and N-cadherin as well as the EMT transcription factor Snail ($P < 0.05$); miR-185 inhibitor showed opposite effects (Fig. 6A). Western blot analysis confirmed these changes: in SGC-7901 cells, miR-185 mimics increased E-cadherin protein expression and decreased Vimentin, N-cadherin and Snail protein expression ($P < 0.05$), while miR-185 inhibitor had the opposite effects (Fig. 6B).

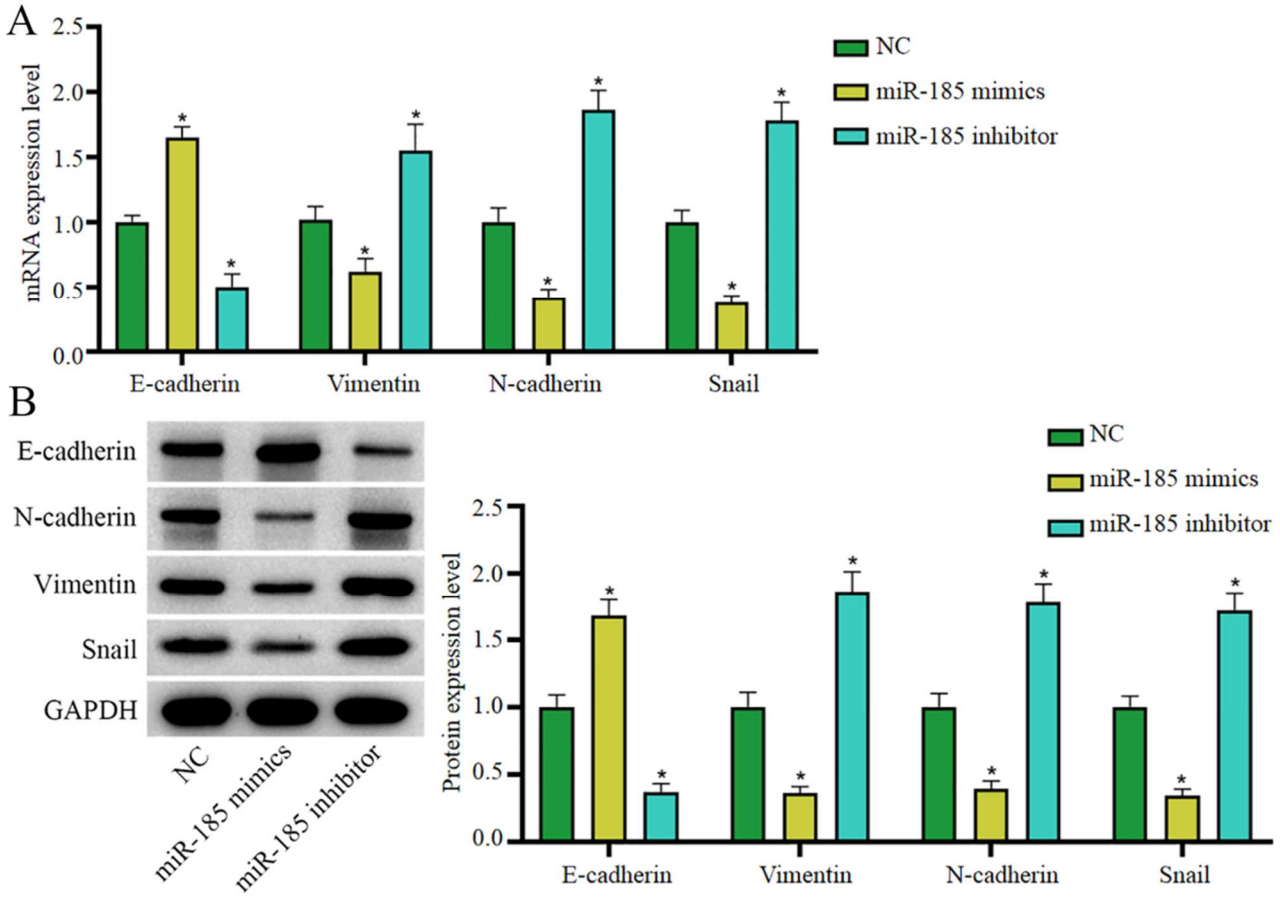

Fig. 6: Effect of miR-185 on epithelial-mesenchymal transition (EMT) in gastric cancer cells.
(A) Real-time quantitative PCR analysis of E-cadherin, Vimentin, N-cadherin, and Snail mRNA expression in SGC-7901 cells. GAPDH was used as an internal control, and expression was normalized to the NC group (set to 1.00); (B) Western blot analysis of E-cadherin, Vimentin, N-cadherin, and Snail protein expression in SGC-7901 cells. GAPDH was used as a loading control. Left panel: representative blots. Right panel: quantitative densitometric analysis. Data are presented as mean ± SD from three independent experiments. One-way ANOVA followed by Tukey's post hoc test was used for comparisons among the three groups (NC, miR-185 mimics, miR-185 inhibitor). *$P < 0.05$ vs. NC group.

miR-185 directly targets CTTN

To determine whether miR-185 directly targets CTTN, binding sites between miR-185 and the CTTN 3'UTR were first predicted using bioinformatics tools (TargetScan and miRDB databases). TargetScan and miRDB predicted a conserved binding site in the CTTN 3‘UTR that is highly complementary to the miR-185 seed region (Fig. 7A). Wild-type (CTTN-3’UTR-WT) and mutant (CTTN-3‘UTR-MUT) dual-luciferase reporter plasmids were constructed. Co-transfection of these plasmids with miR-185 mimics into 293T cells revealed that miR-185 mimics significantly reduced luciferase activity of the CTTN-3’UTR-WT plasmid (inhibition rate 58.0%, $P < 0.05$) but had no effect on the CTTN-3‘UTR-MUT plasmid ($P > 0.05$) (Fig. 7B).

Effect of miR-185 on the Cdc42-N-WASP signaling pathway in gastric cancer cells

Western blot analysis showed that miR-185 mimics significantly downregulated Cdc42 and N-WASP protein expression, whereas miR-185 inhibitor significantly upregulated them ($P < 0.05$) (Fig. 8).

CTTN overexpression rescues miR-185-induced phenotypic changes in gastric cancer cells

To validate whether miR-185 exerts its biological effects through CTTN, a rescue experiment was performed in SGC-7901 cells. Co-transfection of miR-185 mimics with a CTTN overexpression plasmid (pcDNA3.1-CTTN, lacking the 3‘UTR) partially restored the expression of CTTN, Cdc42 and N-WASP, as well as the miR-185 mimics-induced changes in E-cadherin, Vimentin, N-cadherin and Snail (Fig. 9A). Functionally, miR-185 mimics alone significantly inhibited cell proliferation (MTT: A570 decreased from 0.85 ± 0.07 to 0.42 ± 0.05; EdU-positive cell rate decreased from 42.6 ± 3.8% to 18.3 ± 2.5%; both $P < 0.05$) and these effects were significantly reversed by CTTN overexpression (A570 increased to 0.78 ± 0.08; EdU-positive cell rate increased to 38.5 ± 3.2%; both $P < 0.05$) (Figs. 9B and 9C).

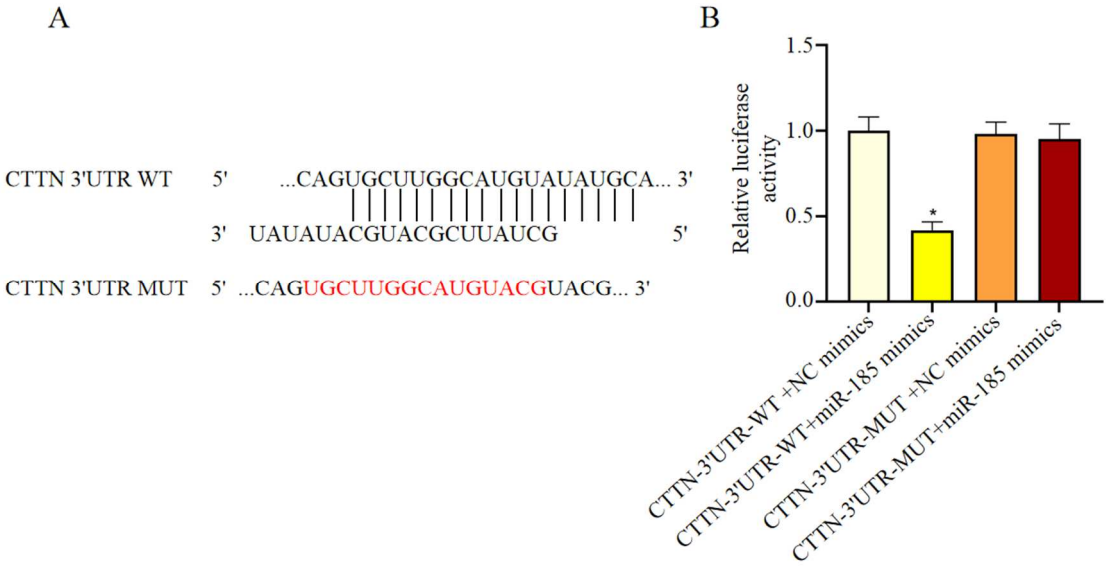

Fig. 7: Dual-luciferase reporter assay confirming CTTN as a direct target of miR-185.
(A) Schematic diagram of the miR-185 binding site in the CTTN 3'UTR. Wild-type (WT) and mutant (MUT) sequences of the binding site are shown; mutations are indicated in red; (B) Dual-luciferase reporter assay. Wild-type (CTTN-3'UTR-WT) or mutant (CTTN-3'UTR-MUT) reporter plasmids were co-transfected into 293T cells with miR-185 mimics or negative controls (NC). Luciferase activity was measured 48 hours after transfection and normalized to the CTTN-3'UTR-WT + NC group (set to 1.00). Data are presented as mean ± SD from three independent experiments. Independent samples t-test was used to compare the miR-185 mimics group with the NC group within each reporter plasmid type. **P* < 0.05 vs. CTTN-3'UTR-WT + NC group; ns, not significant.

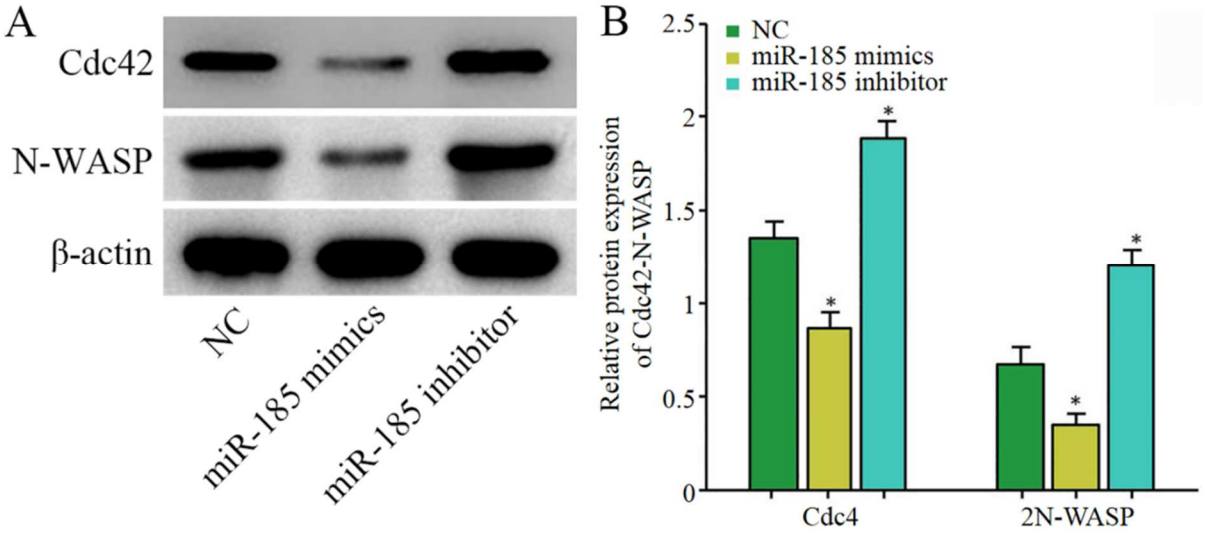

Fig. 8: Effect of miR-185 on the Cdc42-N-WASP signaling pathway in gastric cancer cells.
(A) Representative Western blot images showing protein expression levels of Cdc42 and N-WASP in SGC-7901 cells transfected with NC mimics, miR-185 mimics, or miR-185 inhibitor. β-actin was used as a loading control; (B) Densitometric quantification of Cdc42 and N-WASP protein expression normalized to β-actin.
Western blot analysis of Cdc42 and N-WASP protein expression in gastric cancer cells after modulation of miR-185 expression. Left panel: representative blots. Right panel: quantitative densitometric analysis. Data are presented as mean ± SD from three independent experiments. One-way ANOVA, followed by Tukey's post hoc test, was used to compare the three groups (NC, miR-185 mimics, miR-185 inhibitor). **P* < 0.05 vs. NC group.

Similarly, miR-185 mimics alone significantly induced apoptosis (total apoptosis rate increased from 4.7 ± 1.1% to 25.4 ± 3.1%, $P < 0.05$) and this effect was significantly attenuated by CTTN overexpression (total apoptosis rate decreased to 7.2 ± 1.5%, $P < 0.05$) (Fig. 9D).

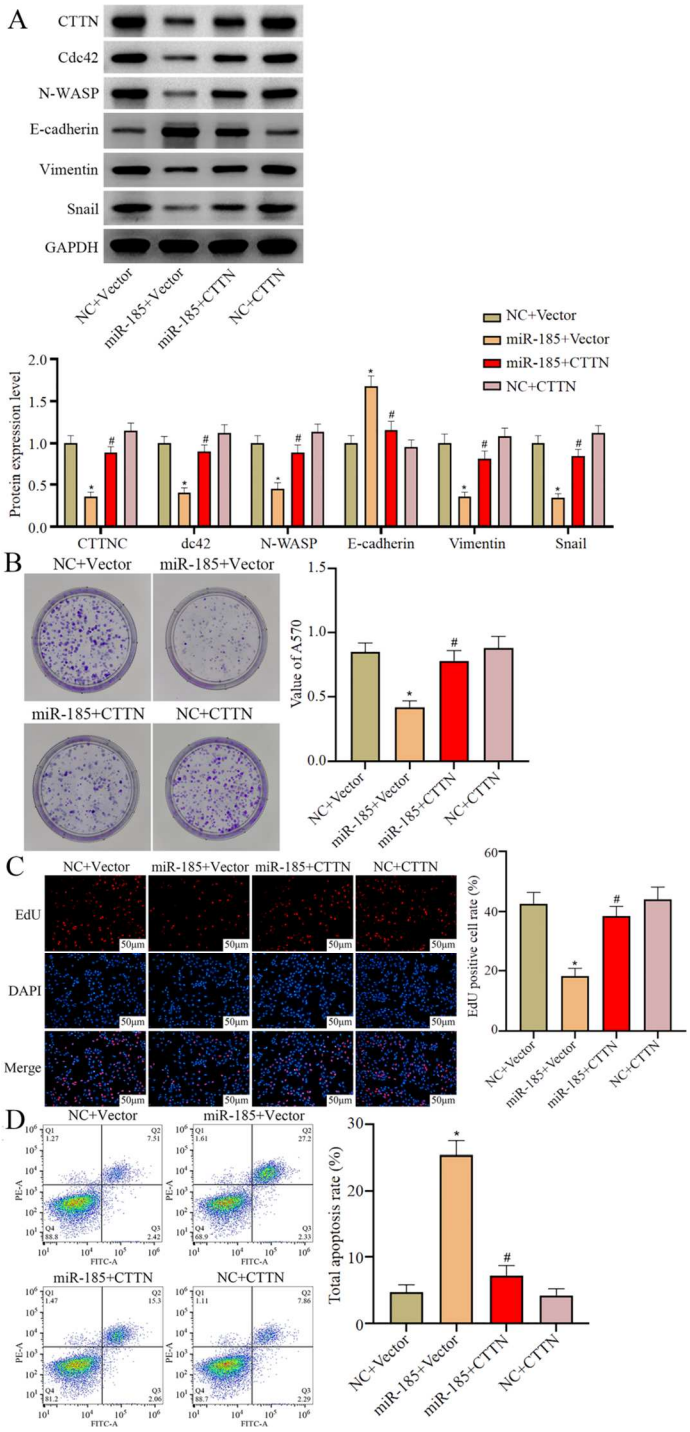

Fig. 9: CTTN overexpression rescues miR-185-induced phenotypic changes in gastric cancer cells.
(A) Western blot analysis of CTTN, Cdc42, N-WASP, E-cadherin, Vimentin, and Snail protein expression. GAPDH was used as a loading control; (B) MTT assay analysis of cell proliferation (A570); (C) EdU incorporation assay analysis of DNA synthesis activity. Left panel: representative fluorescence images (EdU: red; Hoechst: blue). Right panel: quantitative analysis of EdU-positive cell rate. Scale bar = 50 μm; (D) Annexin V/PI double staining flow cytometry analysis of apoptosis. Left panel: representative flow cytometry plots. Right panel: quantitative analysis of total apoptosis rate. Data are presented as mean ± SD from three independent experiments. One-way ANOVA followed by Tukey's post hoc test was used for comparisons among the four groups (NC mimics + Vector, miR-185 mimics + Vector, miR-185 mimics + CTTN, NC mimics + CTTN). **P* < 0.05 vs. NC mimics + Vector group; #P < 0.05 vs. miR-185 mimics + Vector group.

Validation of miR-185 function in AGS gastric cancer cells

To further confirm the generalizability of the findings, key experiments were repeated in the AGS gastric cancer cell line. Real-time quantitative PCR showed that miR-185 expression was significantly increased by miR-185 mimics and decreased by miR-185 inhibitor in AGS cells ($P < 0.05$) (Fig. 10A). CTTN mRNA and protein expression were significantly decreased by miR-185 mimics and increased by miR-185 inhibitor ($P < 0.05$) (Fig. 10B). Western blot analysis confirmed that miR-185 mimics significantly reduced Cdc42 and N-WASP protein levels, whereas miR-185 inhibitor increased them ($P < 0.05$) (Fig. 10C). MTT assay showed that miR-185 mimics significantly inhibited AGS cell proliferation, while miR-185 inhibitor significantly promoted it ($P < 0.05$) (Fig. 10D).

DISCUSSION

As transcriptional regulators, miRNAs are involved in tumorigenesis and progression and can serve as prognostic indicators (Metcalf, 2024). miRNAs are dysregulated in various cancers (Dimitrov *et al*., 2026). Aberrant expression of miR-185 has been observed in multiple tumors, including esophageal, liver and kidney cancers (Wei *et al*., 2024, Khare *et al*., 2022). The role of miR-185 in gastric cancer and its underlying molecular mechanism were assessed and explored in this study. Reduced miR-185 expression was observed in gastric cancer tissues and its clinicopathological associations confirmed correlations with lymph node metastasis and tumor stage. Epithelial-mesenchymal transition (EMT) frequently occurs during gastric cancer progression and plays a critical role in tumor invasion and metastasis. EMT is involved in various cellular processes, including embryonic development, tumor metastasis and inflammation (Li *et al*., 2023, Rendon-Huerta *et al*., 2026). Further investigation showed that upregulating miR-185 inhibited gastric cancer cell proliferation and promoted apoptosis, accompanied by increased E-cadherin and decreased Vimentin expression, suggesting that miR-185 may regulate EMT. Epithelial cells, interconnected through polarity, undergo morphological and phenotypic changes to become mesenchymal cells, a process that drives EMT (Tomecka *et al*., 2024). Studies have confirmed that tumor invasion and metastasis are not only related to EMT but also closely associated with invasive pseudopodia. During tumor cell invasion and metastasis, various pseudopodia can form, including filopodia, lamellipodia and invadopodia (Hao *et al*., 2025). CTTN encodes cortactin, which promotes the binding of microfilament agonist proteins and oncogenic tyrosine kinase v-Src, thereby facilitating tumor cell invasion and metastasis (Nicoletto *et al*., 2024). Cdc42, a member of the Rho family of small GTPases, interacts with switch proteins that regulate the cycling between GTP-bound (active) and GDP-bound (inactive) states, serving as an initiator of intracellular signaling for pseudopodia formation and regulating downstream signaling pathways involved in tumor invasion and metastasis (Kreider-Letterman *et al*., 2023; Xie *et al*., 2023).

The expression characteristics and clinical significance of miR-185 in gastric cancer were clarified in this study. Previous studies on miR-185 in gastric cancer have been limited by small sample sizes. By analyzing 58 gastric cancer tissues and paired adjacent normal tissues, it was confirmed that miR-185 is significantly downregulated in gastric cancer and its low expression correlates with lymph node metastasis and TNM stage. This is consistent with the tumor-suppressive role of miR-185 in other gastrointestinal cancers, such as oral and esophageal cancers (Babaeenezhad *et al*., 2022). CTTN was also identified as a direct target of miR-185 in gastric cancer. While previous studies have shown that miR-185-5p targets TAGLN2 to regulate cisplatin resistance in lung adenocarcinoma (Yu *et al*., 2023) and targets KIF1B to inhibit tumor cell proliferation, migration and invasion in glioma (Guan *et al*., 2022), the direct targeting of CTTN by miR-185 has not been previously validated in gastric cancer. Using bioinformatic prediction, dual-luciferase reporter assays with wild-type and mutant constructs and Western blot analysis, it was demonstrated for the first time that miR-185 directly binds to the 3'UTR of CTTN and negatively regulates its expression. As a cytoskeletal regulatory protein, CTTN plays a key role in pseudopodia formation and invasion/metastasis in gastric cancer cells (Lu *et al*., 2023), providing a new molecular explanation for the tumor-suppressive mechanism of miR-185.

Furthermore, it was revealed that miR-185 regulates the Cdc42-N-WASP signaling pathway through CTTN. Cdc42 plays a critical role in gastric cancer cell migration and invasion. Previous studies have shown that Cdc42 participates in MICAL2-mediated regulation of E-cadherin stability, thereby influencing gastric cancer cell migration (Wang *et al*., 2022b). Previous research demonstrated that in prostate and breast cancers, N-WASP, acting downstream of Cdc42, promotes tumor cell adhesion to endothelial cells and lung metastasis through the regulation of β1-integrin expression (Cerutti et al., 2024). However, whether miR-185 affects this pathway through CTTN has not been reported. It was confirmed by Western blot and rescue experiments that miR-185 inhibits Cdc42 and N-WASP protein expression through targeting CTTN, thereby suppressing gastric cancer cell proliferation, inducing apoptosis and reversing EMT. This discovery links miR-185, CTTN and the Cdc42-N-WASP signaling pathway, offering new insights into the regulatory mechanisms of this pathway in gastric cancer.

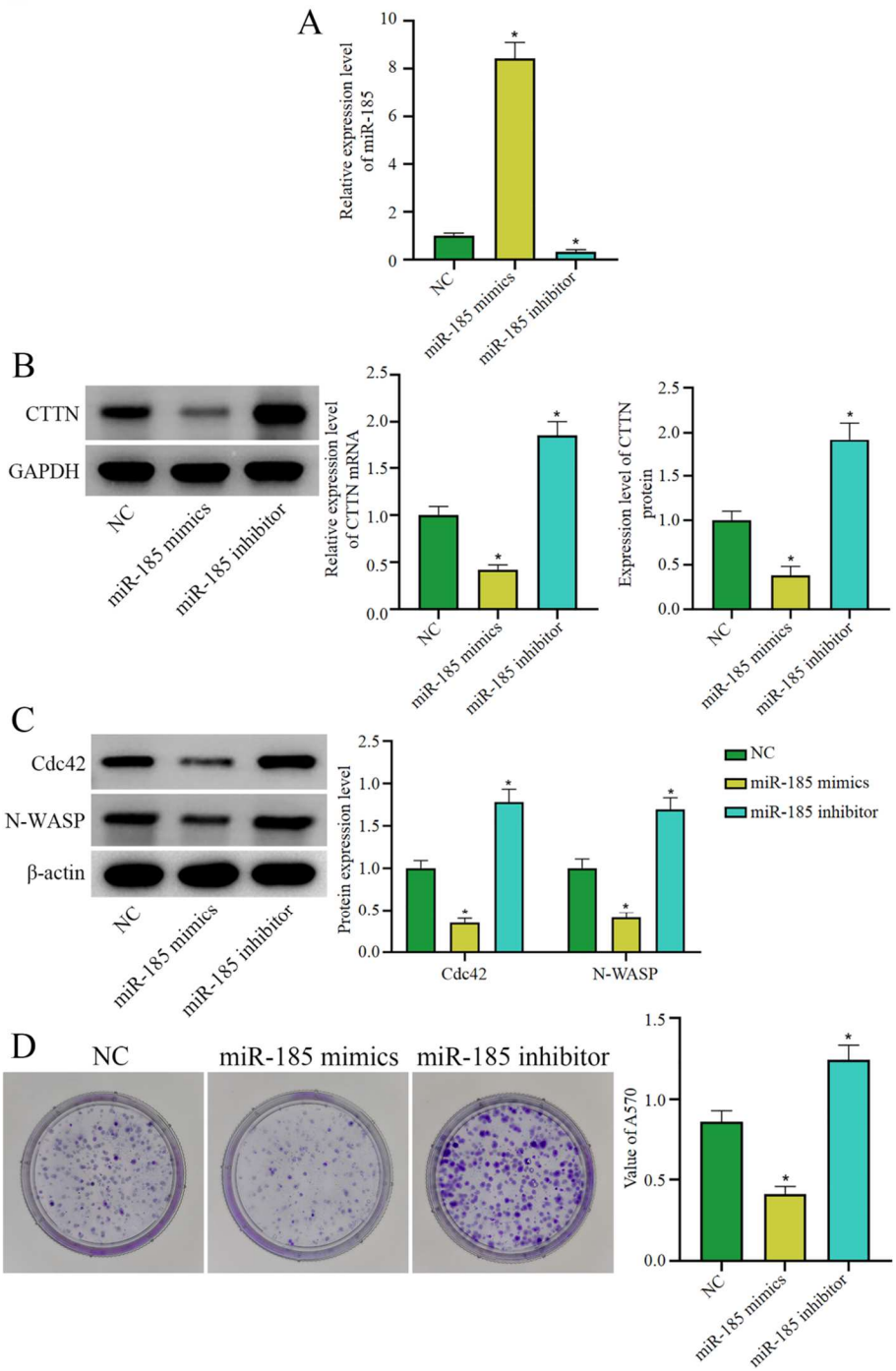

Fig. 10: Validation of miR-185 function in AGS gastric cancer cells.
(A) Real-time quantitative PCR analysis of miR-185 expression in AGS cells after transfection with miR-185 mimics, miR-185 inhibitor, or negative controls (NC). U6 was used as an internal control. Data are presented as mean ± SD from three independent experiments; (B) Effect of miR-185 modulation on CTTN expression in AGS cells. Left panel: real-time quantitative PCR analysis of CTTN mRNA expression. Right panel: Western blot analysis of CTTN protein expression. GAPDH was used as a loading control. Data are presented as mean ± SD from three independent experiments; (C) Western blot analysis of Cdc42 and N-WASP protein expression in AGS cells after transfection. GAPDH was used as a loading control. Data are presented as mean ± SD from three independent experiments; (D) MTT assay analysis of the effect of miR-185 modulation on AGS cell proliferation. Data are presented as mean ± SD from three independent experiments. Independent samples t-test was used for comparisons between two groups (NC vs. miR-185 mimics; NC vs. miR-185 inhibitor).*$P < 0.05$ vs. NC group.

Functional assays demonstrated that upregulation of miR-185 significantly inhibited gastric cancer cell proliferation (consistent results from MTT and EdU assays), induced apoptosis (consistent results from Caspase-3 activity and flow cytometry) and reversed EMT (upregulation of E-cadherin, downregulation of Vimentin, N-cadherin and Snail). The EdU incorporation assay, which directly measures DNA synthesis, corroborated the MTT results, enhancing the reliability of the proliferation data. Annexin V/PI double staining confirmed apoptosis induction and cross-validation across multiple methods strengthened the conclusions. EMT is a critical process by which tumor cells acquire invasive and metastatic capabilities and the inhibitory effect of miR-185 on EMT was confirmed through analysis of multiple EMT markers, including E-cadherin, Vimentin, N-cadherin and Snail. Rescue experiments further demonstrated that CTTN overexpression partially reversed the phenotypic changes induced by miR-185, confirming that CTTN is a key downstream effector of miR-185.

The findings of this study suggest that miR-185 is downregulated in gastric cancer and that its overexpression inhibits tumor cell proliferation, induces apoptosis and reverses EMT, indicating that miR-185 mimics may have therapeutic potential for gastric cancer. Additionally, as a direct target of miR-185, CTTN is highly expressed in gastric cancer and correlates with invasion and metastasis, making it a candidate for small-molecule inhibitors or miR-185-based therapies. However, translating miR-185-based strategies into clinical applications faces several challenges. Naked miRNAs are easily degraded by nucleases in the body and have poor tissue-targeting capabilities (Zhang *et al*.,2025). Current delivery systems, such as lipid nanoparticles (LNPs), exosomes and viral vectors, each have their own limitations (Di *et al*.,2025). Moreover, miRNA mimics may exhibit partial complementarity to the 3′ UTRs of non-target genes, leading to off-target effects and potential toxicity (Xia *et al*., 2025). Although specific binding between miR-185 and CTTN was confirmed by dual-luciferase reporter assay, a comprehensive assessment of off-target effects using transcriptomic profiling or bioinformatic prediction is still needed. All functional experiments in this study were conducted *in-vitro*; animal model studies are lacking and the pharmacokinetics, biodistribution, antitumor efficacy and safety of miR-185 *in-vivo* remain unknown. Future studies should focus on optimizing delivery systems with high tumor specificity and low immunogenicity, comprehensively evaluating off-target effects using RNA sequencing or proteomic analysis and establishing orthotopic xenograft or patient-derived xenograft (PDX) models to systematically assess the in *vivo* antitumor efficacy and safety of miR-185 mimics.

It is important to note that while miR-185 was demonstrated to regulate the Cdc42-N-WASP signaling pathway by targeting CTTN in this study, other possible molecular mechanisms cannot be excluded. First, CTTN may participate in gastric cancer progression through other signaling pathways, such as ERK/FAK or SRF. Second, miR-185 may simultaneously target multiple downstream genes that collectively mediate its effects on gastric cancer cell phenotypes. Bioinformatic predictions suggest that potential targets of miR-185 include several molecules involved in cytoskeletal regulation and signal transduction, such as RhoA and ROCK, whose roles in mediating miR-185's tumor-suppressive effects warrant further investigation. Additionally, the Cdc42-N-WASP signaling pathway may interact with other gastric cancer-related pathways, such as Wnt/β-catenin and PI3K/AKT and these findings may represent only a part of a complex regulatory network.

It is also noteworthy that the normal gastric epithelial cell line GES-1 was included as an in vitro baseline control and it was confirmed that miR-185 expression was significantly lower in SGC-7901 and AGS gastric cancer cells than in GES-1 cells, consistent with the downregulation observed in gastric cancer tissues, consistent with the downregulation observed in gastric cancer tissues. This finding supports the hypothesis that miR-185 may play a tumor-suppressive role in gastric cancer and further enhances the clinical relevance of the in vitro results. However, GES-1 cells are SV40-immortalized and differ from primary normal gastric epithelial cells. Future studies using primary human gastric epithelial cells would provide a more comprehensive characterization of miR-185 expression in gastric cancer.

Several limitations of this study should be acknowledged. The sample size was relatively small (n = 58) and only univariate analysis was performed, without adjustment for confounding factors. *In vitro experiments were limited to two cell lines and in vivo* validation was lacking. Functional validation of the signaling axis was incomplete because Arp2/3 activity and actin polymerization status were not directly assessed. GES-1 cells are immortalized and differ from primary cells. *In-vitro* experiments were repeated only three times, which may limit statistical power. Future studies should include large-scale multicenter cohorts, in vivo animal models and direct measurement of Arp2/3 activity to validate the findings further.

CONCLUSION

This study found that miR-185 expression is downregulated in gastric cancer tissues and that low expression is associated with lymph node metastasis and TNM stage. *In vitro experiments showed that overexpression of miR-185 inhibited gastric cancer cell*

proliferation, induced apoptosis and reversed epithelial-mesenchymal transition, possibly by targeting CTTN and thereby affecting Cdc42 and N-WASP protein expression. These findings suggest that miR-185 may be involved in gastric cancer progression and provide a preliminary experimental basis for further research.

Acknowledgments
This work was supported by the Innovation and Entrepreneurship Training Program for College Students of Heilongjiang Province (No. S202510222084); The Basic Scientific Research Operating Expenses for Higher Education Institutions of Heilongjiang Province (No.23KYYWF0596); The Basic Scientific Research Operating Expenses for Higher Education Institutions of Heilongjiang Province (No. 2022-KYYWF-0620); The Natural Sciece Foundation of Heilongjiang Province, China (No. LH2020H003); Natural Science Foundation Cultivation Program of Jiamusi University, China (No. JMSUGPZR2209); Science Foundation Program of Jiamusi University, China (No. 2023SZDJC002).

Authors' contributions
Da Lian: Conceptualization and design of the study; Chengyao Bai: Performed experiments, data analysis and interpretation, drafted the manuscript; Xiaomeng Zhang: Performed experiments, including cell culture, transfection, real-time quantitative PCR, participated in data analysis and interpretation; Xia Hou: Performed experiments, Western blot, dual-luciferase reporter assay and flow cytometry, participated in data analysis and interpretation; Qingtian Wu: Design of the study, collection of clinical tissue samples and pathological data; Pengyu Xie: Conceptualization, critical revision and review of the manuscript. All authors have read and approved the final version of the manuscript.

Funding
This study was supported by the National Natural Science Foundation of China (Grant No. 32071269) to Feng Wang.

Data availability statement
The datasets generated and/or analyzed during the current study are available from the corresponding author upon reasonable request.

Ethical approval
The use of archived de-identified tissue samples was approved by the ethics committee of Jiamusi University School of Basic Medicine with a waiver of informed consent (Approval No.: 2025-KYYWF-08920). This study was performed in adherence with the STROBE guidelines. See supplementary file for the STROBE checklist.

Conflict of interest
The authors declare no conflict of interest.

Supplementary data

REFERENCES

Babaeenezhad E, Naghibalhossaini F, Rajabibazl M, Jangravi Z, Hadipour Moradi F, Fattahi MD, Hoheisel JD, Sarabi MM and Shahryarhesami S (2022). The Roles of microRNA miR-185 in digestive tract cancers. *Noncoding RNA*., **8**(5): 67.

Bao L, Zhong M, Zhang Z, Yu X, You B, You Y, Gu M, Zhang Q, Chen W, Lei W and Hu S (2024). Stiffness promotes cell migration, invasion and invadopodia in nasopharyngeal carcinoma by regulating the WT-CTTN level. *Cancer Sci.*, **115**(3): 836-846.

Castro-Guijarro AC, Vanderhoeven F, Mondaca JM, Redondo AL, Zoppino FCM, Fernandez-Munoz JM, Sanchez AM and Flamini MI (2022). Combination treatment of retinoic acid plus focal adhesion kinase inhibitor prevents tumor growth and breast cancer cell metastasis. *Cells.*, **11**(19): 2988.

Cerutti C, Lucotti S, Menendez ST, Reymond N, Garg R, Romero IA, Muschel R and Ridley AJ (2024). IQGAP1 and NWASP promote human cancer cell dissemination and metastasis by regulating β1-integrin via FAK and MRTF/SRF. *Cell Rep*., **43**(4): 113989.

Chen L, Yang X, Zhu P, Bao H, Wu Y, Ji K, Zhang J, Wu X, Zhou K, Xu J, Tang J, Wang A and Bu Z (2025). Hepatoid adenocarcinoma of the stomach and non-hepatoid alpha-fetoprotein-producing gastric cancer exhibit a high degree of molecular similarity. *Cell Oncol*., **49**(1): 1.

Chen R, Yao Z and Jiang L (2024). Construction and validation of a TTN mutation associated immune prognostic model for evaluating immune microenvironment and outcomes of gastric cancer: an observational study. *Medicine*., **103**(29): e38979.

Di Ianni E, Obuchi W, Breyne K and Breakefield XO (2025). Extracellular vesicles for the delivery of gene therapy. *Nat Rev Bioeng*., **3**(5): 360-373.

Dimitrov L, Stancheva GS, Kyurkchiyan SG, Mitkova M, Stancheva I, Valcheva S, Komitova K, Skelina S, Rangachev J and Popov TM (2026). Biomarkers of common molecular dysregulation in tumor tissue and peritumor mucosa in head and neck SCC: Insights into field cancerization. *Int J Mol Sci*., **27**(3): 1212.

Fang C, Wang W, Deng JY, Sun Z, Seeruttun SR, Wang ZN, Xu HM, Liang H and Zhou ZW (2018). Proposal and validation of a modified staging system to improve the prognosis predictive performance of the 8th AJCC/UICC pTNM staging system for gastric adenocarcinoma: A multicenter study with external validation. *Cancer Commun (Lond)*., **38**(1): 67.

Guan Y, Yang W, Zhang F, Zhang L and Wang L (2022). CircPOSTN competes with KIF1B for miR-185-5p binding sites to promote the tumorigenesis of glioma. *Brain Res Bull*., **180**: 86–96.

Hao Z, Zhang M, Du Y, Liu J, Zeng G, Li H and Peng X (2025). Invadopodia in cancer metastasis: Dynamics, regulation and targeted therapies. *J Transl Med*., **23**(1): 548.

Hasegawa K, Matsui TK, Kondo J and Kuwako KI (2022). N-WASP-Arp2/3 signaling controls multiple steps of dendrite maturation in Purkinje cells *in-vivo*. *Development.*, **149**(23): dev201214.

Hou M, Li C and Dong S (2021). LINC00963/miR-4458 regulates the effect of oxaliplatin in gastric cancer by mediating autophagic flux through targeting of ATG16L1. *Sci Rep.*, **11**(1): 20951.

Khare S, Khare T, Ramanathan R and Ibdah JA (2022). Hepatocellular carcinoma: The role of microRNAs. *Biomolecules*., **12**(5): 645.

Kreider-Letterman G, Castillo A, Mahlandt EK, Goedhart J, Rabino A, Goicoechea S and Garcia-Mata R (2023). ARHGAP17 regulates the spatiotemporal activity of Cdc42 at invadopodia. *J Cell Biol*., **222**(2): e202207020.

Li D, Xia L, Huang P, Wang Z, Guo Q, Huang C, Leng W and Qin S (2023). Heterogeneity and plasticity of epithelial-mesenchymal transition (EMT) in cancer metastasis: Focusing on partial EMT and regulatory mechanisms. *Cell Prolif*., **56**(6): e13423.

Lu G, Du R, Dong J, Sun Y, Zhou F, Feng F, Feng B, Han Y and Shang Y (2023). Cancer associated fibroblast derived SLIT2 drives gastric cancer cell metastasis by activating NEK9. *Cell Death Dis*., **14**(7): 421.

Metcalf GAD (2024). MicroRNAs: Circulating biomarkers for the early detection of imperceptible cancers via biosensor and machine-learning advances. *Oncogene*., **43**(28): 2135–2142.

Nicoletto RE, Holdcraft CJ, Yin AC, Retzbach EP, Sheehan SA, Greenspan AA, Laugier CM, Trama J, Zhao C, Zheng H and Goldberg GS (2024). Effects of cadherin mediated contact normalization on oncogenic Src kinase mediated gene expression and protein phosphorylation. *Sci Rep*., **14**(1): 23942.

Rendón-Huerta EP, Melendez-Rendón R, Aguilar AS and Montano LF (2026). Do metastatic cells arise from PD-L1+ cell niches in gastric adenocarcinoma?. *Int J Mol Sci*., **27**(4): 1829.

Shahabi A, Naghili B, Ansarin K, Montazeri M, Dadashpour M and Zarghami N (2021). Let-7d and miR-185 impede epithelial-mesenchymal transition by downregulating Rab25 in breast cancer. *Asian Pac J Cancer Prev*., **22**(1): 305–313.

Tian SQ, Shen JJ, Sun DP and Chen WM (2025). lncRNA CHAF1B-2 contributes to the tumorigenesis of gastric cancer by activating the Wnt/β-catenin pathway. *Sci Rep.*, **15**(1): 568.

Tomecka P, Kunachowicz D, Gorczynska J, Gebuza M, Kuźnicki J, Skinderowicz K and Choromanska A (2024). Factors determining epithelial-mesenchymal transition in cancer progression. *Int J Mol Sci*., **25**(16): 8972.

Wei QY, Jin F, Wang ZY, Li BJ, Cao WB, Sun ZY and Mo SJ (2024). MicroRNAs: A novel signature in the metastasis of esophageal squamous cell carcinoma. *World J Gastroenterol*., **30**(11): 1497–1523.

Wang G, Zhang Z and Xia C (2021). Long non-coding RNA LINC00240 promotes gastric cancer progression via modulating miR-338-5p/METTL3 axis. *Bioengineered.*, **12**(2): 9678-9691.

Wang Y, Fang T, Wang Y, Yin X, Zhang L, Zhang X, Zhang D, Zhang Y, Wang X, Wang H and Xue Y (2022a). Impact of AADAC gene expression on prognosis in patients with Borrmann type III advanced gastric cancer. *BMC Cancer*., **22**(1): 635.

Wang Q, Qi C, Min P, Wang Y, Ye F, Xia T, Zhang Y and Du J (2022b). MICAL2 contributes to gastric cancer cell migration via Cdc42-dependent activation of E-cadherin/β-catenin signaling pathway. *Cell Commun Signal*., **20**(1): 136.

Xia C, Cheng L, Zhao W, Chang A, Wang Z, Liu H, Pan X, Li W, Koji S, Li Z, Li B, Wang L and Yu G (2025). LncRNA SYISL promotes fibroblast myofibroblast transition via miR-23a-mediated TRIOBP regulation. *Cell Mol Life Sci*., **82**(1): 214.

Xie W, Han Z, Zuo Z, Xin D, Chen H, Huang J, Zhu S, Lou H, Yu Z, Chen C, Chen S, Hu Y, Huang J, Zhang F, Ni Z, Shen X, Xue X and Lin K (2023). ASAP1 activates the IQGAP1/CDC42 pathway to promote tumor progression and chemotherapy resistance in gastric cancer. *Cell Death Dis*., **14**(2): 124.

Yu N, Gong H, Chen W and Peng W (2023). CircRNA ZKSCAN1 promotes lung adenocarcinoma progression by miR-185-5p/TAGLN2 axis. *Thorac Cancer*., **14**(16): 1467–1476.

Zhang W, Wang L, Demna MY, Xiong J, Luo M, Wang Y and Wang F (2025). Regulatory mechanisms of miRNA turnover: insights into ZSWIM8-mediated target-directed microRNA degradation. *Biomedicines*., **13**(9): 2194.

Zheng S, Qin F, Yin J, Li D, Huang Y, Hu L, He L, Lv C, Li X, Li S and Hu W (2023). Role and mechanism of actin-related protein 2/3 complex signaling in cancer invasion and metastasis: A review. *Medicine (Baltimore)*., **102**(14): e33158.